

UC Merced

UC Merced Previously Published Works

Title

Multi-objective optimal design of sliding mode control with parallel simple cell mapping method

Permalink

<https://escholarship.org/uc/item/9v79x9k1>

Journal

Journal of Vibration and Control, 23(1)

ISSN

1077-5463

Authors

Qin, Zhi-Chang
Xiong, Fu-Rui
Ding, Qian
[et al.](#)

Publication Date

2017

DOI

10.1177/1077546315574948

Peer reviewed

Multi-objective Optimal Design of Sliding Mode Control with Parallel Simple Cell Mapping Method

Journal of Vibration and Control
000(00):1–1
©The Author(s) 2014
Reprints and permission:
sagepub.co.uk/journalsPermissions.nav
DOI:doi number
<http://jms.sagepub.com>


Zhi-Chang Qin and Fu-Rui Xiong and Qian Ding
Department of Mechanics, Tianjin University
Tianjin, 300072, China

Carlos Hernández and Jesús Fernandez and Oliver Schütze
CINVESTAV-IPN, Computer Science Department
Mexico City 07360, Mexico

Jian-Qiao Sun*
School of Engineering, University of California
Merced, CA 95343, USA

Abstract

This paper presents a study of multi-objective optimal design of a sliding mode control for an under-actuated nonlinear system with the parallel simple cell mapping method. The multi-objective optimal design of the sliding mode control involves 6 design parameters and 5 objective functions. The parallel simple cell mapping method finds the Pareto set and Pareto front efficiently. The parallel computing is done on a graphic processing unit (GPU). Numerical simulations and experiments are done on a rotary flexible arm system. The results show that the proposed multi-objective designs are quite effective.

Keywords

Sliding mode control; simple cell mapping; multi-objective optimization; parallel computing; graphic processing unit (GPU)

1. Introduction

Sliding mode control (SMC) is a powerful nonlinear control technique. The basic idea of SMC is to drive the system to a sliding surface, a manifold in the state space, and let the system move along the sliding surface towards the desired steady

* Corresponding author. e-mail: jqsun@ucmerced.edu. Honorary Professor of Tianjin University, China.

state. This paper presents a study of multi-objective optimal design of the sliding mode control and the sliding surface with the help of the parallel cell mapping method.

Many publications have focused on how to design the optimal sliding surfaces and switching terms (Gasimov et al., 2005; Costa et al., 2003; Wu et al., 2010, 2013). The decoupled sliding mode control for high order systems is studied by Lo & Kuo (1998). SMC design with neural network training for multi-objective optimization is considered by Costa et al. (2003). Genetic algorithm based multi-objective optimization on sliding surface construction is studied by Li et al. (1996). Adaptive SMC design using learning algorithms is investigated by Babae & Khosravi (2012). Although only limited studies on multi-objective optimal SMC design are reported in recent years, several successful applications of popular biologically inspired algorithms such the particle swarm optimization (PSO) by Alitavoli et al. (2012) and genetic algorithm (GA) by Sharifi et al. (2012) indicates a growing trend on this topic. Mahmoodabadi et al. (2013) studied the Pareto optimal design of the decoupled sliding mode controller for an inverted pendulum system by comparing the Sigma method (Mostaghim & Teich, 2003), the modified NSGA-II algorithm (Atashkari et al., 2007) and the MOGA toolbox in Matlab with a novel multi-objective PSO algorithm. The multi-objective optimization of SMC design usually aims at determining several free parameters of the controller to meet the performance requirements in time or frequency domain (Al-Dakkan et al., 2003; Sharifi et al., 2012). These performance requirements are often conflicting. Also, the optimization should consider the hardware capability such as saturation and parameter uncertainty, which makes the multi-objective optimal SMC design more challenging and interesting.

Recently, the cell mapping methods originally developed by Hsu in the 1980s for global analysis of nonlinear dynamical systems (Hsu, 1987) are found to be highly effective in discovering the global structure of the Pareto set, the solution of the multi-objective optimization problems (MOPs) (Xiong et al., 2014; Naranjani et al., 2013). The cell mapping methods have been successfully applied to low and moderate dimensional problems and the multi-objective optimal proportional-integral-derivative (PID) control design for linear and nonlinear dynamical systems by Hernández et al. (2013). Furthermore, the cell mapping methods are naturally parallelizable in computing. This paper reports the application of the cell mapping method for MOPs implemented on a graphic processing unit (GPU) with massive parallel processing capability. In particular, we apply the method to the multi-objective optimal design problem of the sliding mode control.

The rest of the paper is organized as follows. We first present the theoretical design of a sliding mode control for an under-actuated two degree of freedom nonlinear system. Stabilities of the control and the sliding surface are considered in Section 2. We then apply the parallel simple cell mapping method for multi-objective optimal design of the sliding mode control with 6 design parameters and 5 performance objectives in Section 2. The parallel cell mapping method is implemented on an NVIDIA GPU with CUDA architecture. Section 4 discusses the numerical and experimental results. Section 5 concludes the paper.

2. Sliding Mode Control Formulation

The experimental apparatus of a rotary flexible joint system produced by Quanser is shown in Figure 1. A base module carrying a rotary flexible link is mounted on a load gear of the SRV02 system driven by a direct current (DC) motor. Two springs attached to the link provide flexibility and introduce geometric nonlinearity to the system. There are plenty of researches on sliding mode control design of smart beam with uncertainties (Li et al., 2011; Gu et al., 2008; Song et al., 1995). However, reports on multi-objective optimal design of sliding mode controller on smart structures are few.

With the Lagrangian method, the nonlinear governing equations of the system can be obtained,

$$\begin{cases} \dot{x}_1 = x_3 \\ \dot{x}_2 = x_4 \\ \dot{x}_3 = f_1(\mathbf{x}) + B_1 u \\ \dot{x}_4 = f_2(\mathbf{x}) + B_2 u \end{cases} \quad (1)$$

where nonlinear functions $f_1(\mathbf{x})$ and $f_2(\mathbf{x})$ are given by

$$f_1(\mathbf{x}) = a_1x_2 + b_1x_3 + c_1x_2^3, \quad (2)$$

$$f_2(\mathbf{x}) = a_2x_2 + b_2x_3 + c_2x_2^3, \quad (3)$$

The coefficients in the above equations as well as B_1 and B_2 are system parameters listed in Table 1. $\mathbf{x} = [x_1, x_2, \dot{x}_1, \dot{x}_2]^T$ is the state vector. x_1 is the angular position of the platform, x_2 is the angular position of the link relative to the base module, and u is the control input. The control objective of this system is to minimize the angular vibration x_2 of the flexible link when the base angle x_1 follows a given tracking command $x_{1d}(t)$. The rotary flexible joint system is an under-actuated nonlinear multi-body system.

2.1. Sliding Mode Control and Stability

Define the tracking error of the two states as

$$\begin{cases} e_1(t) = x_1(t) - x_{1d}(t), \\ e_2(t) = x_2(t) - x_{2d}(t), \end{cases} \quad (4)$$

where $x_{1d}(t)$ and $x_{2d}(t)$ are the desired reference trajectories for $x_1(t)$ and $x_2(t)$. Define a sliding surface $s(t)$ as a linear combination of the tracking errors (Ashrafiuon & Erwin, 2008)

$$s(t) = \alpha_a \dot{e}_1(t) + \lambda_a e_1(t) + \alpha_u \dot{e}_2(t) + \lambda_u e_2(t). \quad (5)$$

where α_a , λ_a , α_u and λ_u are the parameters defining the sliding surface. These parameters will be determined later in the paper.

On the sliding surface, we impose $s(t) = 0$ and $\dot{s}(t) = 0$.

$$\begin{aligned} \dot{s}(t) &= \alpha_a \ddot{e}_1(t) + \lambda_a \dot{e}_1(t) + \alpha_u \ddot{e}_2(t) + \lambda_u \dot{e}_2(t) \\ &= \alpha_a f_1(\mathbf{x}) + \alpha_u f_2(\mathbf{x}) + [\alpha_a B_1 + \alpha_u B_2] u + \lambda_a x_3(t) + \lambda_u x_4(t) - \rho_d(t) \\ &= 0, \end{aligned} \quad (6)$$

where $\rho_d(t) = \alpha_a \ddot{x}_{1d}(t) + \alpha_u \ddot{x}_{2d}(t) + \lambda_a \dot{x}_{1d}(t) + \lambda_u \dot{x}_{2d}(t)$. From the above equation, we can obtain the equivalent control as

$$u_{eq} = -\sigma [\alpha_a f_1(\mathbf{x}) + \alpha_u f_2(\mathbf{x}) + \lambda_a x_3(t) + \lambda_u x_4(t) - \rho_d(t)], \quad (7)$$

where

$$\sigma = \frac{1}{\alpha_a B_1 + \alpha_u B_2}. \quad (8)$$

We introduce the robust control law with a switching term as,

$$u = u_{eq} + u_{sw} = -\sigma [\alpha_a \hat{f}_1(\mathbf{x}) + \alpha_u \hat{f}_2(\mathbf{x}) + \lambda_a x_3(t) + \lambda_u x_4(t) - \rho_d(t) + K \text{sign}(s)], \quad (9)$$

where $\hat{f}_1(\mathbf{x})$ and $\hat{f}_2(\mathbf{x})$ are the estimates of $f_1(\mathbf{x})$ and $f_2(\mathbf{x})$. We assume that the estimation error of the nonlinear functions are bounded,

$$\begin{aligned} |f_1(\mathbf{x}) - \hat{f}_1(\mathbf{x})| &\leq F_{s_1}, \\ |f_2(\mathbf{x}) - \hat{f}_2(\mathbf{x})| &\leq F_{s_2}. \end{aligned} \quad (10)$$

where $F_{s_1} = 0.75 |x_1^3 + x_2^3|$ and $F_{s_2} = 0.5 |x_1^3 + x_2^3|$ are the known positive functions. These bounds are determined based on an assumption that the linear portions of the system model in Equations (2) and (3) are accurate, while the nonlinear terms have uncertainties in the coefficients c_1 and c_2 . The numerical values in the bounds are estimated based on the measurement of the system geometries. Define a Lyapunov function in terms of the sliding surface,

$$V(\mathbf{x}, \dot{\mathbf{x}}) = \frac{1}{2} s^2(t). \quad (11)$$

Hence, we have

$$\begin{aligned} \dot{V}(\mathbf{x}, \dot{\mathbf{x}}) &= s(t)\dot{s}(t) \\ &= s(t) \{ \alpha_a f_1(\mathbf{x}) + \alpha_u f_2(\mathbf{x}) + [\alpha_a B_1 + \alpha_u B_2] u + \lambda_a x_3(t) + \lambda_u x_4(t) - \rho_d(t) \} \\ &= s(t) \left[\alpha_a (f_1(\mathbf{x}) - \hat{f}_1(\mathbf{x})) + \alpha_u (f_2(\mathbf{x}) - \hat{f}_2(\mathbf{x})) - K \text{sign}(s(t)) \right] \\ &\leq (\alpha_a F_{s_1} + \alpha_u F_{s_2} - K) |s(t)| \\ &\leq -\eta |s(t)|, \end{aligned} \quad (12)$$

where $K = \alpha_a F_{s_1} + \alpha_u F_{s_2} + \eta$ and $\eta > 0$ is a positive number. The control is thus stable with this choice of K . In the tracking problem of the rotary flexible joint, we have $x_{1d} = 1$, $x_{2d} = 0$, $\dot{x}_{1d} = 0$, $\dot{x}_{2d} = 0$ and thus $\rho_d(t) = 0$.

In the real time implementation, we introduce the saturation function $\text{sat}(\frac{s}{\phi})$ to replace the sign function $\text{sign}(s)$ to avoid high frequency chattering. The saturation function is given by

$$\text{sat} \left(\frac{s(t)}{\phi} \right) = \begin{cases} 1, & s(t) > \phi \\ \frac{s(t)}{\phi}, & -\phi < s(t) < \phi, \quad \phi > 0 \\ -1, & s(t) < -\phi \end{cases} \quad (13)$$

where $0 < \phi < 1$ is the boundary layer thickness for the switching term of the control. The stability of the control with the saturation function can be proven in the same manner. We shall omit the details of the proof here.

2.2. Stability on the Sliding Surface

In order for the system to sliding down to the origin, the sliding surface must be stable. On the sliding surface, $s(t) = \alpha_a \dot{e}_1(t) + \lambda_a e_1(t) + \alpha_u \dot{e}_2(t) + \lambda_u e_2(t) = 0$. Hence, $\dot{e}_1(t)$ can be solved from this equation as

$$\dot{e}_1(t) = \delta_1 e_2(t) + \delta_2 \dot{e}_2(t) + \delta_3 e_1(t), \quad (14)$$

where

$$\delta_1 = -\frac{\lambda_u}{\alpha_a}, \delta_2 = -\frac{\alpha_u}{\alpha_a}, \delta_3 = -\frac{\lambda_a}{\alpha_a}. \quad (15)$$

Making use of the equivalent control u_{eq} of Equation (7) and noting that $\ddot{e}_2 = \dot{x}_4 - \dot{x}_{2d} = \dot{x}_4$, we obtain

$$\begin{aligned}\ddot{e}_2 &= f_2(\mathbf{x}) + B_2 \{-\sigma [\alpha_a f_1(\mathbf{x}) + \alpha_u f_2(\mathbf{x}) + \lambda_a x_3(t) + \lambda_u x_4(t)]\} \\ &= \sigma (\xi_1 x_2 + \xi_2 x_3 + \xi_3 x_4 + \xi_4 x_2^3),\end{aligned}\quad (16)$$

where

$$\begin{aligned}\xi_1 &= \alpha_a a_2 B_1 - \alpha_u a_1 B_2, \\ \xi_2 &= \alpha_a b_2 B_1 - \alpha_u b_1 B_2 - \lambda_a B_2, \\ \xi_3 &= -\lambda_u B_2, \\ \xi_4 &= \alpha_a c_2 B_1 - \alpha_u c_1 B_2.\end{aligned}\quad (17)$$

Since $x_{1d} = 1$, $\dot{x}_{1d} = 0$, and $x_{2d} = \dot{x}_{2d} = 0$, we have $e_2 = x_2$, $\dot{e}_1 = x_3$ and $\dot{e}_2 = x_4$. Equation (16) reads

$$\begin{aligned}\ddot{e}_2 &= \sigma [\xi_1 e_2(t) + \xi_2 \dot{e}_1(t) + \xi_3 \dot{e}_2(t) + \xi_4 e_2^3(t)] \\ &= \sigma \left\{ \xi_1 e_2(t) + \xi_2 \left[-\frac{\lambda_a}{\alpha_a} e_1(t) - \frac{\lambda_u}{\alpha_a} e_2(t) - \frac{\alpha_u}{\alpha_a} \dot{e}_2(t) \right] + \xi_3 \dot{e}_2(t) + \xi_4 e_2^3(t) \right\} \\ &= \beta_1 e_2(t) + \beta_2 \dot{e}_2(t) + \beta_3 e_1(t) + \sigma \xi_4 e_2^3(t),\end{aligned}\quad (18)$$

where

$$\begin{aligned}\beta_1 &= \sigma \left\{ [a_2 B_1 - a_1 B_2] \alpha_a + [b_1 B_2 - b_2 B_1] \lambda_u + B_2 \frac{\lambda_a \lambda_u}{\alpha_a} \right\}, \\ \beta_2 &= \sigma \left\{ [b_1 B_2 - b_2 B_1] \alpha_u - B_2 \lambda_u + B_2 \frac{\lambda_a \alpha_u}{\alpha_a} \right\}, \\ \beta_3 &= \sigma \left\{ [b_1 B_2 - b_2 B_1] \lambda_a + B_2 \frac{\lambda_a^2}{\alpha_a} \right\}.\end{aligned}\quad (19)$$

Define a set of new state variables as $\mathbf{y} = [y_1, y_2, y_3]^T = [e_2(t), \dot{e}_2(t), e_1(t)]^T$. The equations for the new state variables can be written as

$$\begin{aligned}\dot{y}_1 &= y_2, \\ \dot{y}_2 &= \beta_1 y_1 + \beta_2 y_2 + \beta_3 y_3 + \sigma \xi_4 y_1^3(t), \\ \dot{y}_3 &= \delta_1 y_1 + \delta_2 y_2 + \delta_3 y_3.\end{aligned}\quad (20)$$

The equilibrium of the new state is $y_1 = y_2 = y_3 = 0$. Linearizing the state equations at the equilibrium, we obtain

$$\begin{aligned}\dot{y}_1 &= y_2, \\ \dot{y}_2 &= \beta_1 y_1 + \beta_2 y_2 + \beta_3 y_3, \\ \dot{y}_3 &= \delta_1 y_1 + \delta_2 y_2 + \delta_3 y_3.\end{aligned}\quad (21)$$

The characteristic equation of the linearized system reads

$$s^3 + \mu_1 s^2 + \mu_2 s + \mu_3 = 0, \quad (22)$$

where s is the Laplace variable, and

$$\begin{aligned} \mu_1 &= -(\beta_2 + \delta_3), \\ \mu_2 &= (\delta_3 \beta_2 - \beta_1 - \delta_2 \beta_3), \\ \mu_3 &= \delta_3 \beta_1 - \delta_1 \beta_3. \end{aligned} \quad (23)$$

The Hurwitz stability conditions lead to

$$\begin{aligned} \mu_1 &> 0, \quad \mu_2 > 0, \\ \mu_3 &> 0, \quad \mu_1 \mu_2 > \mu_3. \end{aligned} \quad (24)$$

In terms of the original system parameters, the stability conditions of the sliding surface read

$$\alpha_a > \alpha_u, \quad \lambda_a > \lambda_u, \quad \frac{\lambda_a}{\alpha_a} > \frac{\lambda_u}{\alpha_u}. \quad (25)$$

A note on the value of σ in Equation (8) is in order. In this work, we have $B_1 = -B_2 > 0$. The first inequality constraint in Equation (25) implies $0 < \sigma < \infty$.

2.3. Multi-objective Optimal Design

The control performance and stability are determined by six parameters: $\mathbf{k} = [\alpha_a, \lambda_a, \alpha_u, \lambda_u, \eta, \phi]$. We now consider the selection of these parameters to meet the following five control objectives of the closed-loop system. Some of the objectives are conflicting to each other.

The first objective t_{p,x_1} is the peak time of the rotary angle x_1 of the base. The second one is the overshoot of this angle defined as $M_{p,x_1} = \frac{|\max(x_1) - x_{1d}|}{x_{1d}} \times 100\%$. These two objectives are conflicting. They are the typical performance metrics for tracking a step input.

The third objective is the maximum amplitude $\max |x_2|$ of the swing angle x_2 of the flexible link. Since the control intends to make the flexible link behave like a rigid connection, this objective function is needed.

Finally, we consider two integrated absolute tracking errors of x_1 and x_2 , defined as

$$\begin{aligned} IAE_{x_1} &= \int_0^T |x_1(t) - x_{1d}(t)| dt, \\ IAE_{x_2} &= \int_0^T |x_2(t) - x_{2d}(t)| dt, \end{aligned} \quad (26)$$

where T is the time when the response reaches the steady state. In this study, we set the time as $T = 5s$. This implies that we are only interested in the responses that settle in 5 seconds or less. Our previous studies suggest that the integrated tracking error plays a compromising role in the optimization (Xiong et al., 2014; Naranjani et al., 2013).

The multi-objective optimal design problem of the sliding mode control with respect to the parameters $\mathbf{k} = [\alpha_a, \lambda_a, \alpha_u, \lambda_u, \eta, \phi]$ can be written as,

$$\min_{\mathbf{k} \in Q} \mathbf{F} = \min_{\mathbf{k} \in Q} \{t_{p,x_1}, M_{p,x_1}, \max |x_2|, IAE_{x_1}, IAE_{x_2}\}, \quad (27)$$

where

$$Q = \{\mathbf{k} \in \mathbf{R}^6 \mid \mathbf{h}(\mathbf{k}) = \mathbf{0}, \mathbf{g}(\mathbf{k}) \leq \mathbf{0}\} \quad (28)$$

$\mathbf{h}(\mathbf{k}) = \mathbf{0}$ and $\mathbf{g}(\mathbf{k}) \leq \mathbf{0}$ denote various equality and inequality constraints in vector format.

3. Parallel Simple Cell Mapping Algorithm

The parallel simple cell mapping (SCM) algorithm is a recently developed numerical method for solving MOPs. The algorithm consists of five parts.

1. Create the cell state space and evaluate the objective functions $\mathbf{F}(\mathbf{k})$ at the cell center \mathbf{k} in the design space.
2. Construct one step cell mappings with the objective functions $\mathbf{F}(\mathbf{k})$ and an MOP search algorithm.
3. Identify periodic cells in the simple cell mapping.
4. Subdivide the periodic cells if refinement is needed, and repeat steps 1 to 3.
5. Carry out the dominance check of the periodic cells.

When constructing the one step simple cell mappings, we use the gradient-free search algorithm (Xiong et al., 2014). The gradient-free search examines the cells in the neighborhood of a pre-image cell by comparing their objective function values. The maximally dominant cell in the neighborhood is chosen as the image cell. The ‘‘maximum dominancy’’ is defined by the biggest norm of the function value differences between the pre-image cell and its neighborhood cells. Hence, this construction of simple cell mappings mimics the steepest descent search, and is implemented in a parallel computing framework.

The constraints are imposed when the mappings are constructed. Recall that the simple cell mapping represents each cell by its center. Hence we judge whether a cell violates the constraints by examining the cell center against the constraints. Once a cell is found to violate a constraint, we mark the cell as a sink cell, which maps to itself (Hsu, 1987).

The global information of the Pareto set is contained in the one step simple cell mappings. The unraveling approach due to Hsu (1987) is used to extract the Pareto set represented by the periodic cells. The unraveling algorithm is originally sequential. We have developed a parallel implementation of the unraveling algorithm.

The dominance check of the periodic cells is usually done sequentially and represents a significant computational effort. This work makes use of a parallel dominance check algorithm as well as the sub-division to refine the cells for improved accuracy (Mahmoodabadi et al., 2013; Sun, 2013; Naranjani et al., 2013). The parallel dominance check simply utilizes the definition of the Pareto set, which states that no cell in the Pareto set dominates another. The dominance check of each cell is conducted by comparing it to the rest of the candidate cells in the set. If a cell is found to be dominated by another cell, we mark it, but don’t delete it from the set. Hence, the size of the set for dominance check is fixed so that the check can be done in parallel starting from many cells at the same time. The output of dominance check contains an indicator array of the dominated cells.

The simple cell mapping method for MOP requires heterogenous programming taking advantages of the host CPU and the parallel computing device GPU. The parallel portions of the computing in the cell creation, mapping construction, unraveling algorithm, dominance check and sub-divisions are executed on GPU. All the rest of the program is executed on CPU.

4. Numerical and Experimental Results

To apply the parallel simple cell mapping method for multi-objective optimal design of the sliding mode control, we select the ranges of the parameters \mathbf{k} as,

$$Q = \{\mathbf{k} \in [0, 2] \times [0, 10] \times [0, 2] \times [0, 2] \times [20, 100] \times [0.3, 1] \subset \mathbf{R}^6 \quad (29)$$

$$| \text{subject to constraint Equation (25)} \}. \quad (30)$$

We also impose the following constraints on the objectives as,

$$[t_{p,x_1}, M_{p,x_1}, \max |x_2|, IAE_{x_1}, IAE_{x_2}] \leq [1.5s, 20\%, 0.2rad, 0.4, 0.05] \quad (31)$$

The initial partition of the design space is $5 \times 5 \times 5 \times 5 \times 5 \times 5 = 5^6$ resulting in 15625 cells. The centers of these cells represent the candidate design vectors \mathbf{k} . For each design vector, we first check the stability of the resulting sliding mode control. If it is stable, we simulate the closed-loop tracking response of the system in Equation (1) with this control. If it is unstable, we discard this design vector. From the time histories of the response, we then identify or compute the objective functions defined in Equation (27).

We have found 145 cells to represent the Pareto set. Each cell in the Pareto set is sub-divided twice into 729 (3^6) smaller cells. The final cell partition of the design space is therefore 45^6 . The refined solution of the Pareto set contains 8165 smaller cells. The parallel computing is conducted with the NVIDIA GeForce GTX 780Ti graphic card which has 2880 CUDA cores and 863MHz base clock rate. The total GPU time of the optimization takes 760s. The Pareto set and Pareto front of the multi-objective optimal design of the sliding mode control are shown in Figures 2 and 3.

To demonstrate the performance of the optimal design, we select 4 points evenly distributed on the Pareto front. These four designs from the Pareto set listed in Table 2 are otherwise random and represent various compromises of the control. The associate objective function values are listed in Table 3. Figure 4 shows the numerical simulations in time domain of the 4 selected control designs. Figure 5 presents the sliding surfaces and control signals. Good tracking and stabilizing performance are achieved.

The experimental hardware consists of the rotary flexible joint module (top) and the SRV02 motor module (bottom) shown in Figure 1, a q-pid data acquisition card, a single channel amplifier, and two encoders for the angle measurement. The real-time control is implemented with the SIMULINK Toolkit of MATLAB 2007 and the QUARC 2.0 by Quanser. We configured the real-time solver as discrete with a fixed-step sample time $t_s = 0.001s$. The amplitude and frequency of the reference square wave are set as 20° and $0.1Hz$.

Figures 6 to 9 show the experimental results of tracking control of the flexible link following the command of the square wave. Figures 10 to 13 show the sliding surfaces and the control signals of the experiment. The same optimal designs considered in the numerical simulations are used in the experiments. The excellent agreement between simulation and experimental results indicates the quality of the modeling of the system as well as the ability of the optimally designed sliding mode control.

5. Concluding Remarks

In this paper, we have applied the parallel cell mapping method for MOPs to design the sliding mode control to meet multiple objectives. The sliding mode control is designed for the under-actuated multi-body mechanical system and is applied to the flexible rotary arm system. Five control performance objectives are introduced to formulate the MOP. Six design parameters that determine the sliding surface shape, switching gain and boundary layer thickness are the design variables. The Pareto set and Pareto front are obtained with the parallel simple cell mapping method. The time domain

simulations and experiments of the selected optimal designs in the Pareto set show good temporal performance of the closed-loop system, and demonstrate the effectiveness of the proposed multi-objective optimal design.

6. Acknowledgements

This work was supported by the Natural Science Foundation of China through the grants (11172197 and 11332008), by the Natural Science Foundation of Tianjin through a key-project grant, and by the UC MEXUS-CONACyT through the project “Cell-to-cell Mapping for Global Multi-objective Optimization”. The second author (FRX) would like to thank the China Scholarship Council (CSC) for sponsoring his study in the United States of America.

References

- Al-Dakkan K. A., et al. (2003). A multi-objective sliding mode approach for the energy saving control of pneumatic servo systems. In Proceedings of ASME International Mechanical Engineering Congress & Exposition, vol. 10, pp. 133–140, Washington, DC., United states.
- Alitavoli M., et al. (2012). Pareto design of sliding-mode tracking control of a biped robot with aid of an innovative particle swarm optimization. In Proceedings of International Symposium on Innovations in Intelligent Systems and Applications, pp. 1–5, Trabzon, Turkey.
- Ashrafiuon H. & Erwin R. S. (2008). Sliding mode control of underactuated multibody systems and its application to shape change control. *International Journal of Control* 81(12):1849–1858.
- Atashkari K., et al. (2007). Modelling and multi-objective optimization of a variable valve-timing spark-ignition engine using polynomial neural networks and evolutionary algorithms. *Energy Conversion and Management* 48(3):1029–1041.
- Babae H. & Khosravi A. (2012). Multi-objective COA for Design Robust Iterative Learning Control via Second-Order Sliding Mode. *International Journal of Control Science and Engineering* 2(6):143–149.
- Costa M. A., et al. (2003). Training neural networks with a multi-objective sliding mode control algorithm. *Neurocomputing* 51:467–73.
- Gasimov R. N., et al. (2005). A nonlinear programming approach for the sliding mode control design. *Applied Mathematical Modelling* 29(11):1135–1148.
- Gu H., et al. (2008). Chattering-free fuzzy adaptive robust sliding-mode vibration control of a smart flexible beam. *Smart Materials and Structures* 17(3):035007.
- Hernández C., et al. (2013). Simple Cell Mapping Method for Multiobjective Optimal PID Control Design. *International Journal of Dynamics and Control* 1(3):231–238.
- Hsu C. S. (1987). *Cell-to-Cell Mapping, A Method of Global Analysis for Nonlinear Systems*. Springer-Verlag, New York.
- Li L., et al. (2011). Adaptive fuzzy sliding mode based active vibration control of a smart beam with mass uncertainty. *Structural Control and Health Monitoring* 18(1):40–52.
- Li Y., et al. (1996). Genetic algorithm automated approach to the design of sliding mode control systems. *International Journal of Control* 63(4):721–39.
- Lo J.-C. & Kuo Y.-H. (1998). Decoupled fuzzy sliding-mode control. *IEEE Transactions on Fuzzy Systems* 6(3):426–435.
- Mahmoodabadi M. J., et al. (2013). Pareto optimal design of the decoupled sliding mode controller for an inverted pendulum system and its stability simulation via Java programming. *Mathematical and Computer Modelling* 57(5-6):1070–1082.
- Mostaghim S. & Teich J. (2003). Strategies for finding good local guides in multi-objective particle swarm optimization (MOPSO). In Proceedings of IEEE Swarm Intelligence Symposium, pp. 26–33.
- Naranjani Y., et al. (2013). A Hybrid Algorithm for the Simple Cell Mapping Method in Multi-objective Optimization. In Proceedings of EVOLVE 2013 - A Bridge between Probability, Set Oriented Numerics, and Evolutionary Computing, Leiden, The Netherland.
- Sharifi M., et al. (2012). Optimization of Sliding Mode Control for a Vehicle Suspension System via Multi-objective Genetic Algorithm with Uncertainty. *Journal of Basic and Applied Scientific Research* 2(7):6724–6729.

- Song G., et al. (1995). A sliding-mode based smooth adaptive robust controller for friction compensation. In Proceedings of Proceedings of the 1995 American Control Conference, vol. 5, pp. 3531–3535.
- Sun J. Q. (2013). Multi-objective Optimal Control Design with the Simple Cell Mapping Method. In Proceedings of ASME International Mechanical Engineering Congress & Exposition, pp. IMECE2013–65506, San Diego, California.
- Wu L., et al. (2010). State Estimation and Sliding-Mode Control of Markovian Jump Singular Systems. *IEEE Transactions on Automatic Control* 55(5):1213–1219.
- Wu L., et al. (2013). Dissipativity-Based Sliding Mode Control of Switched Stochastic Systems. *IEEE Transactions on Automatic Control* 58(3):785–791.
- Xiong F.-R., et al. (2014). Multi-objective optimal design of feedback controls for dynamical systems with hybrid simple cell mapping algorithm. *Communications in Nonlinear Science and Numerical Simulation* 19(5):1465–1473.

Table 1. Parameters of the rotary flexible joint system.

Parameter	Value	Parameter	Value
a_1	628.5625	a_2	-1024.7473
b_1	-40.4033	b_2	40.4033
c_1	-665.5048	c_2	1084.9745
B_1	61.7567	B_2	-61.7567

Table 2. The control parameters of the four selected Pareto points.

Case	α_a	λ_a	α_u	λ_u	η	ϕ
a	0.4667	8.3333	0.3333	0.3333	33.3330	0.7433
b	1.0000	9.6667	0.7333	1.9333	33.3330	0.7433
c	0.8667	9.0000	0.6000	0.2000	54.6670	0.4167
d	0.8667	9.6667	0.6000	0.2000	44.0000	0.9767

Table 3. The objective function values of the four selected Pareto points.

Case	t_{p,x_1} (s)	M_{p,x_1} (%)	$\max x_2 $ (rad)	IAE_{x_1}	IAE_{x_2}
a	0.4375	2.5322	0.1131	0.1852	0.0297
b	1.1850	0.0002	0.0837	0.2480	0.0177
c	0.7650	0.0131	0.1583	0.1775	0.0318
d	0.8400	0.0085	0.1008	0.1994	0.0238

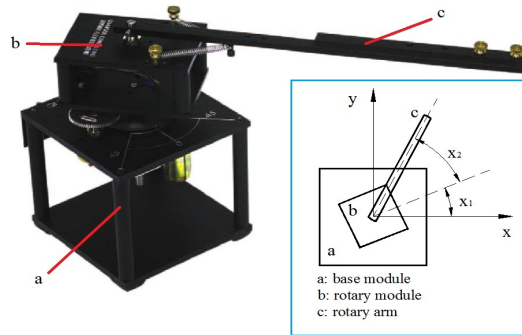


Fig. 1. The rotary flexible joint experimental setup made by Quanser.

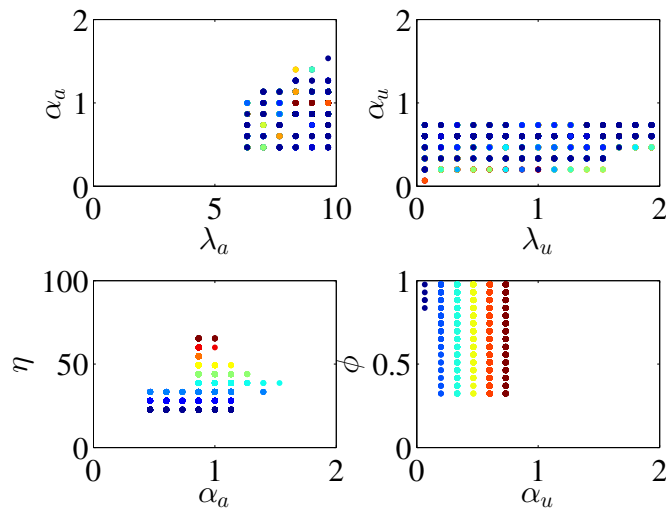


Fig. 2. The 6-dimensional Pareto set of the optimal sliding mode control design, projected on to the 2-dimensional sub-space of the design parameters. The Pareto set contains 8165 cells. The color code indicates the level of λ_u , ϕ , λ and α_u in each subplot from upper left in counterclockwise order. The Pareto set provides a wide range of choices in the 6-dimensional parameter space.

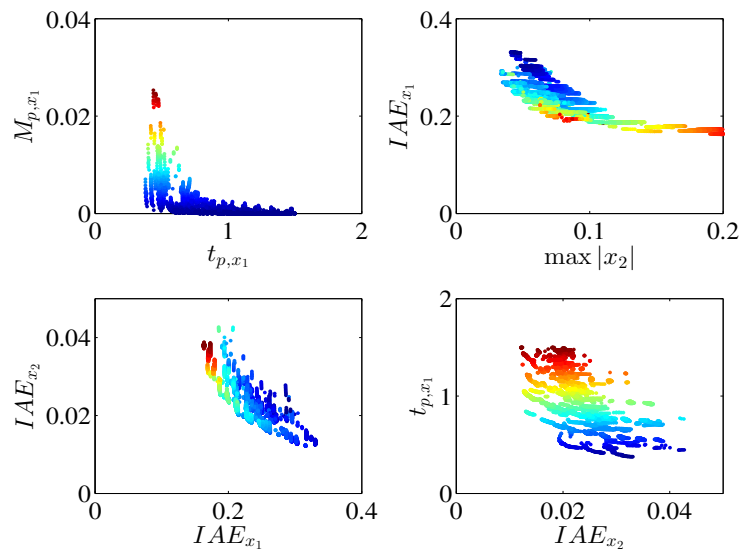


Fig. 3. The 5-dimensional Pareto front of the objective functions, projected on to 2-dimensional sub-spaces of the objective space. The color code indicates the level of M_{p,x_1} , IAE_{x_2} , $\max |x_2|$ and t_{p,x_1} in subplots from upper left in counterclockwise order. The conflicting nature among these objectives can be observed clearly. For example, the overshoot and peak time are conflicting for tracking control, which can be seen in the upper left plot.

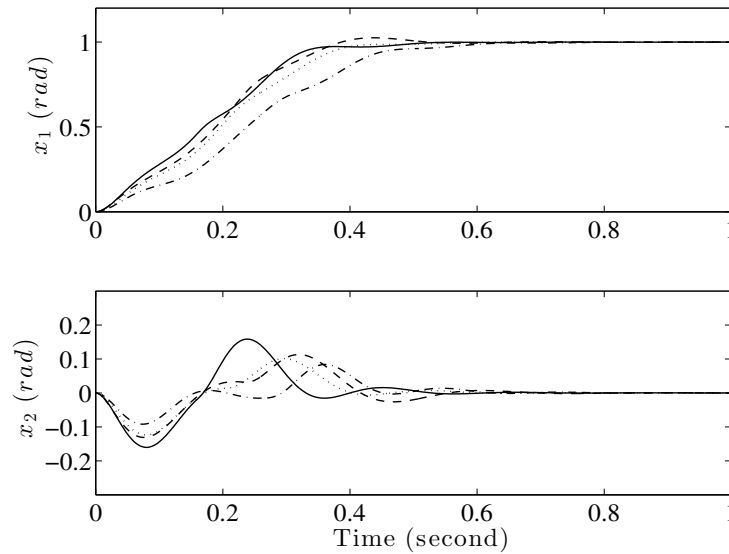


Fig. 4. Simulation results of the base angle x_1 (top) and the angle of the flexible link x_2 (bottom) with the 4 selected Pareto optimal control designs. The dash line, dot-dash line, solid line and dotted line correspond to cases a to d in Table 2.

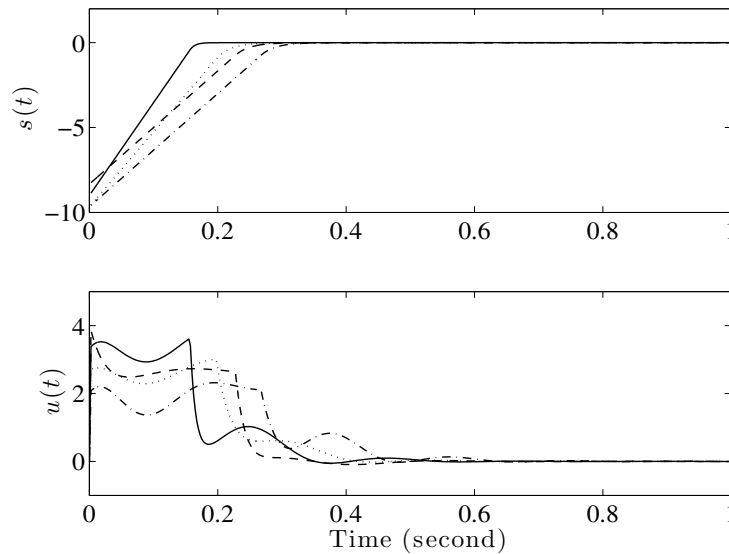


Fig. 5. The sliding surface $s(t)$ and control signal $u(t)$ with the 4 selected Pareto optimal designs. The dash line, dot-dash line, solid line and dotted line correspond to cases a to d in Table 2.

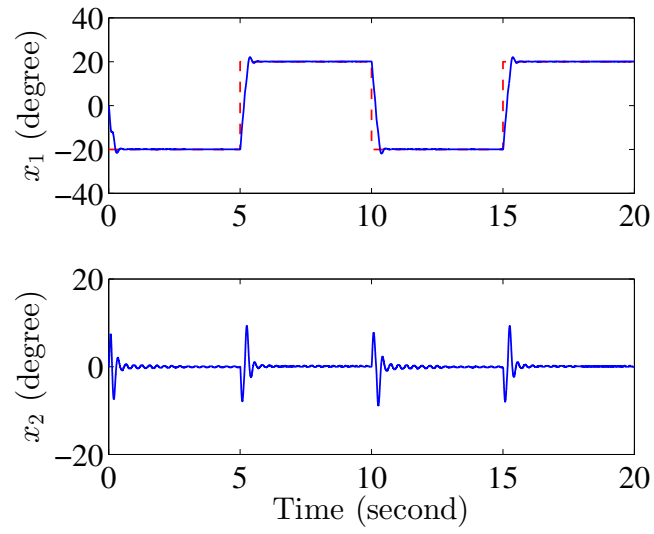


Fig. 6. Experimental square wave tracking response of the rotary flexible joint under the sliding mode control with the Pareto optimal design of case *a* in Table 2. x_1 is the base angle and x_2 is the angle of the flexible link.

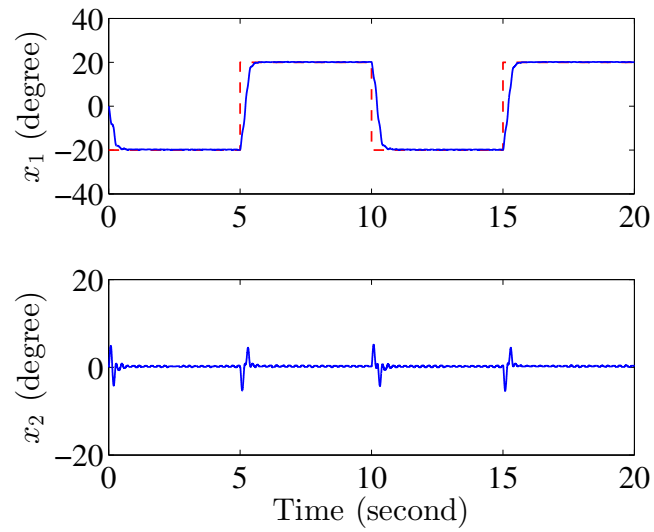


Fig. 7. Experimental square wave tracking response of the rotary flexible joint under the sliding mode control with the Pareto optimal design of case *b* in Table 2.

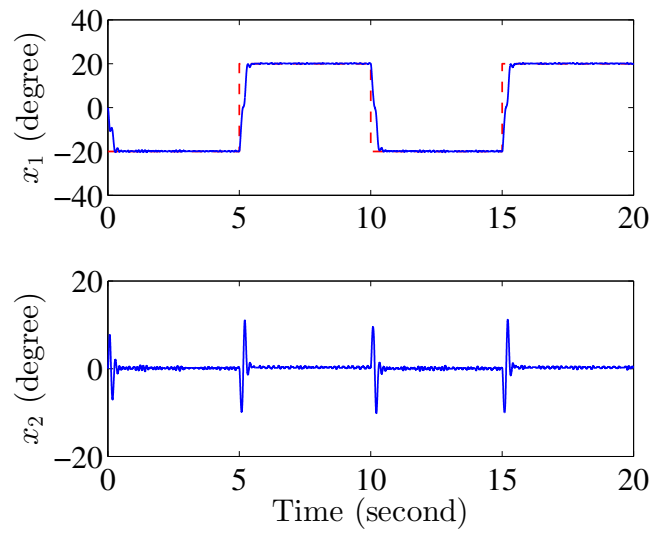


Fig. 8. Experimental square wave tracking response of the rotary flexible joint under the sliding mode control with the Pareto optimal design of case *c* in Table 2.

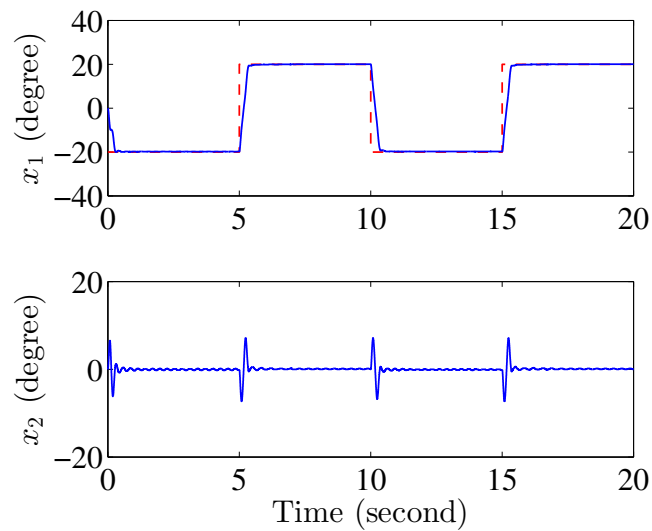


Fig. 9. Experimental square wave tracking response of the rotary flexible joint under the sliding mode control with the Pareto optimal design of case *d* in Table 2.

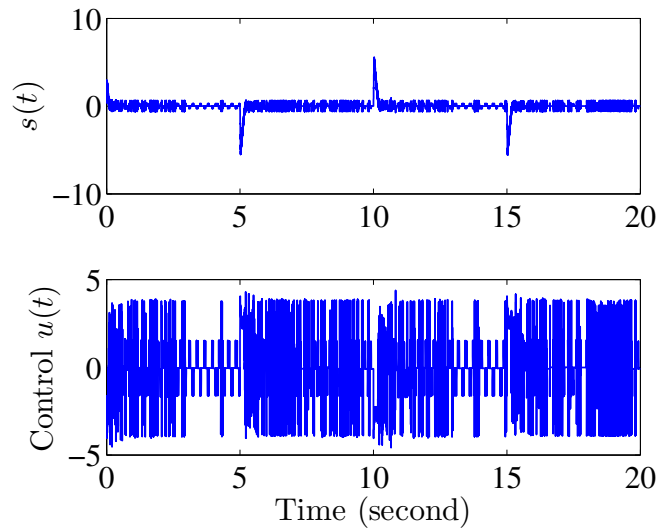


Fig. 10. The sliding surface $s(t)$ and control signal $u(t)$ of the rotary flexible joint experiment with the Pareto optimal design of case a in Table 2.

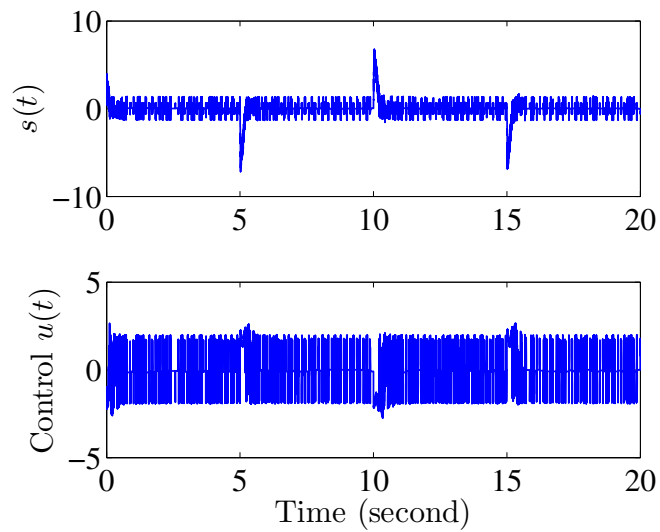


Fig. 11. The sliding surface $s(t)$ and control signal $u(t)$ of the rotary flexible joint experiment with the Pareto optimal design of case b in Table 2.

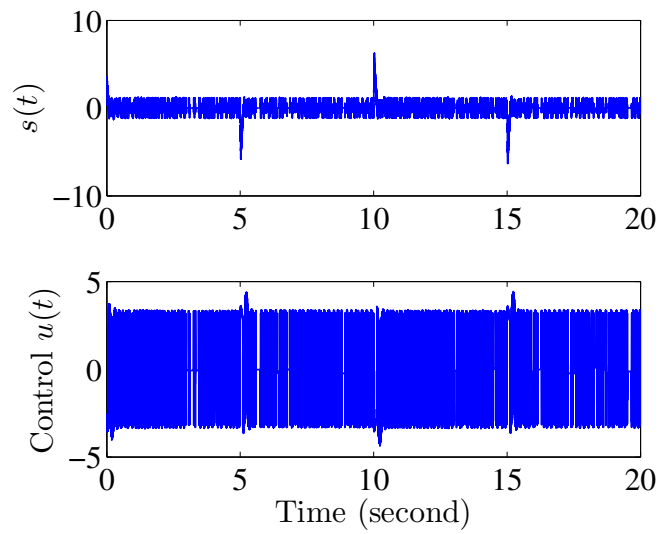


Fig. 12. The sliding surface $s(t)$ and control signal $u(t)$ of the rotary flexible joint experiment with the Pareto optimal design of case c in Table 2.

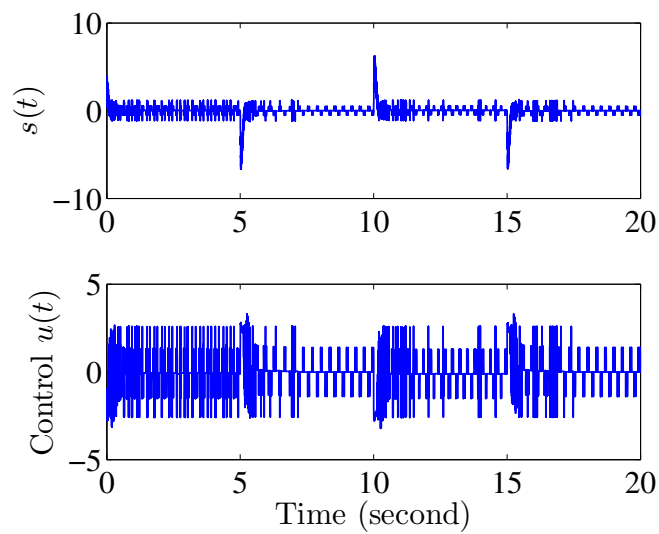


Fig. 13. The sliding surface $s(t)$ and control signal $u(t)$ of the rotary flexible joint experiment with the Pareto optimal design of case d in Table 2.